


Article

# Intelligent Radio Frequency Identification for URLLC in Industrial IoT Networks

Tiantian Zhang <sup>1,2</sup> , Pinyi Ren <sup>1,2,\*</sup>, Dongyang Xu <sup>1,2</sup> and Zhanyi Ren <sup>1,2</sup>

<sup>1</sup> School of Information and Communications Engineering, Xi'an Jiaotong University, Xi'an 710049, China; tiantianzhang@stu.xjtu.edu.cn (T.Z.); xudongyang@xjtu.edu.cn (D.X.); ren12852@stu.xjtu.edu.cn (Z.R.)

<sup>2</sup> Shaanxi Smart Networks and Ubiquitous Access Research Center, Xi'an 710049, China

\* Correspondence: pyren@mail.xjtu.edu.cn

**Abstract:** In the era of Industry 4.0, there are many emerging industrial Internet of Things (IIoT) applications that require ultrareliable and low-latency communications (URLLCs), such as time-sensitive networking (TSN), status reporting, and remote control. With the deployment of massive intelligent devices in IIoT networks, providing security for device physical-layer access is a challenging issue, especially for URLLC applications with strict latency and reliability constraints. We thus developed an intelligent radio frequency identification (RFI) framework to provide a lightweight and energy-efficient physical-layer access scheme for URLLCs via leveraging unique hardware-level imperfections of transmitter. We propose a novel semisupervised-learning (SSL) algorithm to realize intelligent RFI in URLLCs scenarios. One-dimensional network construction is also exploited to improve the accuracy of the proposed SSL algorithm. On the basis of the proposed RFI framework, we analyze the overall uplink transmission error probability and network availability of URLLCs with massive MIMO, which can achieve comparable symmetry performance with that of downlink, and experimental evaluation is also provided to gain comprehensive insight on RFI. Numerical and experimental results demonstrate the effectiveness of our proposed RFI framework and the impact of channel correlation, and provide design guidelines for supporting the radio frequency identification of URLLC applications in IIoT systems.

**Keywords:** URLLCs; industrial IoT; symmetry; intelligent radio frequency identification; semisupervised learning; short-packet communication



**Citation:** Zhang, T.; Ren, P.; Xu, D.; Ren, Z. Intelligent Radio Frequency Identification for URLLC in Industrial IoT Networks. *Symmetry* **2022**, *14*, 801. <https://doi.org/10.3390/sym14040801>

Academic Editors: Hanguan Shan, Howard Hao Yang and Atef Abdrabou

Received: 15 March 2022

Accepted: 9 April 2022

Published: 12 April 2022

**Publisher's Note:** MDPI stays neutral with regard to jurisdictional claims in published maps and institutional affiliations.



**Copyright:** © 2022 by the authors. Licensee MDPI, Basel, Switzerland. This article is an open access article distributed under the terms and conditions of the Creative Commons Attribution (CC BY) license (<https://creativecommons.org/licenses/by/4.0/>).

## 1. Introduction

In the era of Industry 4.0, the industrial Internet of Things (IIoT) has attracted extensive attention from industrial companies and academics [1–4]. Compared to conventional wired control systems, the IIoT utilizes wireless networks to decentralize and improve efficiency during various industrial processes with massive sensors and other devices [5]. The standardization and commercialization of fifth-generation (5G) wireless networks produced various mission-critical IoT applications requiring ultrareliable and low-latency communications (URLLCs), such as autonomous driving, target tracking, and tactile Internet [6–10]. The third-generation partnership project (3GPP) has standardized general URLLC requirements, with 99.999% reliability and about 1–10 ms latency with short packet transmission. In fact, there are several emerging URLLC applications in IIoT networks, such as time-sensitive networking (TSN), status reporting, and remote control [11,12].

Nonetheless, it is extremely challenging for URLLCs to simultaneously ensure latency and reliability due to their stringent and conflicting constraints such as the fading and propagation loss of channel [13–15]. Multiuser channel access, coexistence, and mutual interference with other systems reduce network availability. Finite block length is the main transmission type, which is different from classical Shannon capacity theory [16,17]. In the existing technical route, multiple upper-layer transfers are often used to confirm

the legitimacy of device access. Unfortunately, traditional security methods rely on pre-defined protocols that require huge communication and computational payloads [5]. A profound security challenge in physical-layer authentication is how to keep it scalable and reliable with low overheads towards future URLLC use, such as industrial scenarios, autonomous vehicles, and edge computing [18–21]. Intelligent radio frequency identification via semisupervised learning (RFISSL) is an emerging physical-layer authentication technique that employs unique device-specific hardware-level features, such as phase noise, inphase/quadrature (I/Q) imbalance, frequency offset, and harmonic distortions [22–26]. It is a potential solution to reduce system overhead under critical applications. Furthermore, how to significantly improve the transmission efficiency of RFI-aided URLLCs is a meaningful topic. Diversity technology is a remarkable technical scheme to improve the efficiency of wireless communication systems. However, the time diversity of uplink transmission is limited in low latency. Frequency diversity is unlikely achievable due to the limitation of terminal standardization. Massive multiple-input multiple-output (MIMO) is achieved by equipping base stations (BSs) with numerous antennas to support multitude user equipment (UE) [16,17]. Massive MIMO can provide remarkable spectral efficiency and reliability benefiting from spatial diversity [13,16]. Furthermore, the transmission block length and the propagation model of URLLCs are assumed to be infinity and an independent fading model, respectively [27,28].

Those assumptions above are not applicable to URLLC practical applications. There is a lack of a strong theoretical foundation of RFI-aided URLLCs with massive MIMO to achieve intelligent physical security and high reliability. On the basis of these assumptions and potential usage scenarios, we present a typical system for Industry 4.0, as shown in Figure 1, which integrates RFI and massive MIMO, where multiple distributed BSs are deployed to cooperatively serve all devices. A central controller is deployed for control and planning to which all BSs are connected by optical or wired cables.

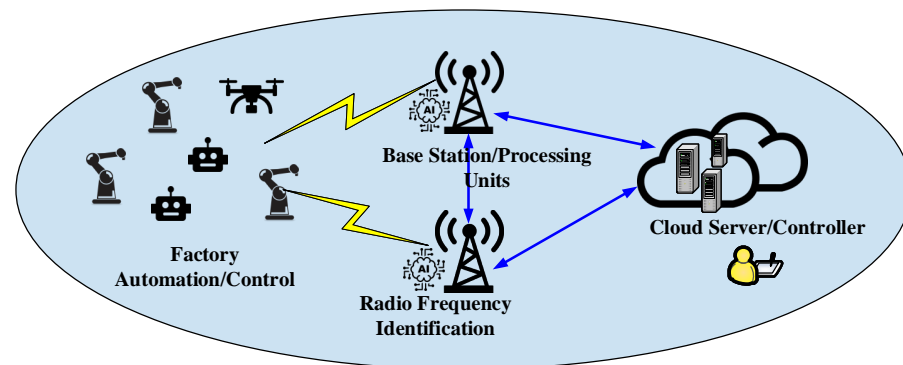


**Figure 1.** Detailed illustration of a typical RFI-aided intelligent automated factory scenario.

### 1.1. Related Works

Recent studies related to URLLCs mainly include short-packet analysis [14], resource allocation [12], massive MIMO, and joint power and placement optimization [9]. Critical reliability and latency were recently investigated in [11] by utilizing Euclidean norm theory. Unlike the vast majority of studies on URLLCs, which focus on the aforementioned single central cell, the authors in [13] applied a cell-free framework into a URLLC system to improve the system sum rate by using a new path-following algorithm. Specifically, the authors in [16] considered a typical massive MIMO scenario that encompasses pilot contamination and imperfect channel state information, which was an early rigorous framework to evaluate uplink transmission error probability and network availability with finite block length. In [5], the authors proposed a one-stage approach radio access to support safety-related industrial applications without a complex high-layer protocol. To improve transmission efficiency, the joint optimization of pilot overhead and power was considered in [17], while the downlink performance of MIMO-NOMA was investigated in [28]. To

sum up, all those methods need additional overload to achieve authentication by higher protocols. There is a lack of systematic analysis for channel correlation impact in URLLC massive MIMO. Therefore, establishing a highly reliable and lightweight access method is a critical problem in URLLCs due to the huge communication payload of conventional protocols. A key guarantee for URLLCs to improve transmission efficiency and access reliability is radio frequency identification by machine learning.

Different from traditional random access schemes, novel physical-layer access based on RFI refers to the accurate identification of different devices. The authors in [19] proposed a nonparametric Bayesian method to classify Zigbee devices. Device fingerprinting and the potential application of wireless security was systematically considered in [22]. The influence of wireless channels to RFI on the Defence Advanced Research Project Agency dataset was investigated in [23]. Gritsenko et al. [24] proposed a novel approach that detects a new device without retraining the network. Jian et al. [25] researched the depth of the model structure and partial equalization. Peng et al. [26] designed a hybrid and adaptive scheme that weighted different features. In [21,29], the application of RFI in physical-layer authentication was discussed to improve efficiency and robustness. Although deep convolutional neural networks (DCNNs) have achieved many remarkable results, they still require massive numbers of labeled samples to guarantee the convergence of the DCNN model [30]. Semisupervised learning (SSL) based on meta pseudo labels is efficient for achieving remarkable identification accuracy. This framework contains two different networks from which to learn by generating soft labels among unlabeled samples. It achieves remarkable identification accuracy in practical applications. This is the first work, to the best of our knowledge, involving the RFI scheme into URLLCs to provide better transmission efficiency and robustness.

### 1.2. Motivations and Contributions

With the rapid development of IIoT, a reliable and low-complexity authentication scheme guarantees that URLLCs can be widely used and deployed. The transmission efficiency of critical mission applications is considered to be an urgent problem. However, traditional higher-protocol access schemes require additional overload, which reduces transmission efficiency. Furthermore, there is a lack of systematic analysis for channel correlation impact in URLLC massive MIMO. Therefore, establishing a highly reliable and lightweight access method is a critical problem in URLLCs with MIMO, and radio frequency identification can be a remarkable solution for physical-layer access via leveraging unique hardware-level impairments. However, traditional supervised learning requires large-scale labeled samples and cannot efficiently learn distributed features. Semisupervised learning (SSL) can achieve remarkable identification accuracy by utilizing meta pseudo labels with few labeled samples and many unlabeled samples. To address this challenge of RFI-aided URLLCs, we utilized RFI and massive MIMO to improve transmission efficiency with low error probability and high availability. The contributions of this paper are summarized as follows.

- We propose a general framework of RFI-aided URLLCs with massive MIMO to further improve uplink transmission efficiency with low error probability and high availability. The key idea is using the physical-layer access scheme instead of the conventional high-layer protocol scheme by RFI. In the proposed framework, we utilize RFISSL to achieve reliable physical access and reduce overload. To the best of our knowledge, this is the first attempt to involve RFI into URLLCs.
- For the proposed RFI, in a typical scenario, we constructed an SSL model on the basis of meta pseudo labels to improve identification accuracy and robustness. We first constructed a novel one-dimensional ResNet model to achieve identification by raw radio frequency (RF) time signals. Due to feedback learning, only a small proportion of the labeled data was needed to achieve excellent performance.
- For a typical short packet transmission scenario, we established a rigorous model with massive MIMO. Saddle-point approximation was applied to characterize system

reliability. Then, the error probability and network achievability of uplink transmission are investigated with finite block length. Furthermore, we evaluate the impact of channel correlation on network availability. Experimental and numerical results demonstrate that RFI-aided URLLCs can achieve high-efficiency transmission and robustness. Lastly, thanks to the generality and robustness of radio frequency identification, the proposed RFI framework can be applied to, for example, physical-layer security, sensing, and localization.

### 1.3. Outline and Notations

The remainder of this paper is organized as follows. In Section 2, the general system model is introduced in detail. Then, the novel architecture of RFI based on SSL is investigated in Section 3. Section 4 outlines mathematical framework performance analysis of RFI-aided URLLCs with massive MIMO. Section 5 investigates the experimental and simulation results to verify the performance of proposed RFI-aided URLLCs with massive MIMO. Lastly, in Section 6, conclusions are drawn in detail.

In this paper, lowercase bold letters denote vector; uppercase bold letters denote matrices;  $(\cdot)^{-1}$ ,  $(\cdot)^*$ ,  $(\cdot)^T$  denote the inverse, conjugate and transpose, respectively;  $\mathcal{CN}(0, \sigma^2)$  denotes a typical Gaussian distribution noise of channel;  $\sigma^2$  denotes variance in Gaussian distribution;  $\|\cdot\|$  denotes the spectral norms of a matrix;  $Q(\cdot)$  represents the Gaussian  $Q$  function;  $\mathbb{E}[\cdot]$  denotes the expectation operator;  $\mathbb{P}[\cdot]$  denotes the probability of a variable; and  $\log(\cdot)$  represents the normal natural logarithm.

## 2. System Model Description

In this section, we introduce an RFI-aided URLLC architecture as shown in Figure 2, where a radio frequency identification model and URLLC system with massive MIMO are deployed to cooperatively serve large-scale smart devices [13]. Massive intelligent devices such as lightweight sensors, robots, and low-power communication devices transmit key information to distributed BSs through wireless channels. Then, received signals are processed by those BSs for high-level information extraction. Furthermore, valuable information is transferred to the cloud server for further computation, analysis, and decision making. Under classical URLLC scenarios, most of the information block is short packages that contain different transmission characteristics compared to typical Shannon capacity theory. We discuss those characteristics in the following section. All those radio frequency characteristics are created in the transmitter, and can be efficiently and completely detected at the receiver side. Once we obtain the device's raw radio frequency signals, authentication processing can be carried out for the access legitimacy of the device.

In order to describe the generation mechanism of RF radio frequency characteristics, the typical structure of the transmitter is shown in Figure 2. All original bits are processed through modulation, upconversion, filtering, and high-power amplification at the transmitting end, and all those radio frequency signals are then transmitted to BSs through antennas [23]. For modulation, some IQ mismatches bring a special nonlinearity. Filtering and high-power amplification modules are key elements for RF signal noise reduction and transmission. The nonlinear characteristics of those different units are embedded in a wireless signal waveform [31–33]. After propagation through a wireless channel, the receiver can obtain raw large-scale RF time signals by directly sampling. When a transmission arrives at BS, device identification is applied to achieve efficient physical-layer access without any additional bit overhead by the RFI system. As shown in the lower right part of Figure 2, the RFI system mainly contains offline training and online evaluation. An offline training process guarantees remarkable identification accuracy with novel construction and a few labeled samples [34]. Supervised learning is the traditional method for model training. However, a number of labeled samples are required. Semisupervised learning is an emerging efficient framework for practical model training due to its self-feedback learning. Furthermore, model construction is a bottleneck for RFI. So, we propose novel one-dimensional model RFIResNet for practical applications. Training parameters

such as batch size, learning ratio, and optimizer are important for training convergence. When trained model is obtained, it is deployed at BSs or edge nodes to achieve radio frequency identification.

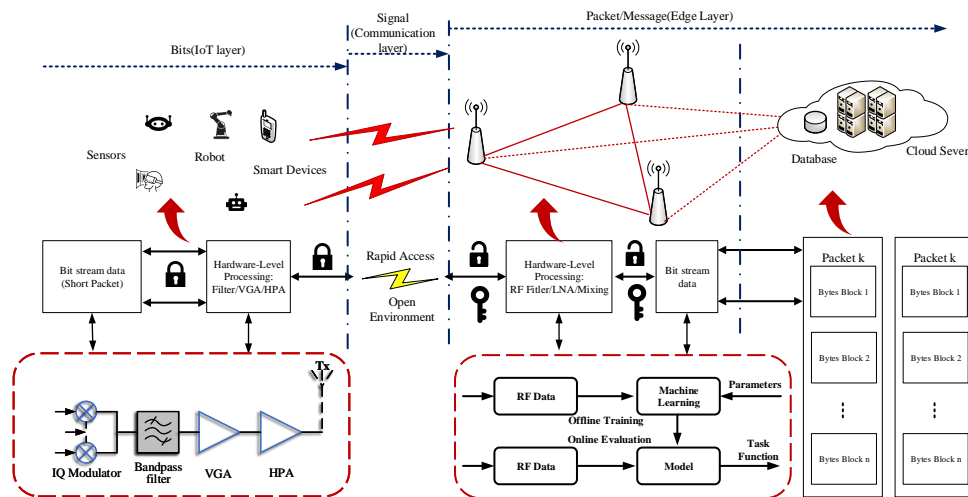


**Figure 2.** Typical architecture of industrial URLLC systems with intelligent RFI to allow for seamless integration of short-packet communication and reliable physical-layer access.

Then, online legitimacy testing is provided to check the information transmission block [35]. Once legitimacy is confirmed, it is transmitted to subsequent processing units for further demodulation and decoding. A central unit is deployed in the cloud sever for computing and controlling to which all BSs are connected by wired cables. Then, high-level decision making and analysis are realized through the central controller in the cloud sever. The considered URLLC system consists of  $N$  smart devices and  $B$  BSs. The number of antennas at the  $b$ -th BSs is  $M_b$ . For simplicity but without loss of generality, we assumed that all those devices were equipped with a single antenna, a central BS with MIMO, and additive Gaussian channel noise.

### 3. RFI Based on Semisupervised Learning For URLLCs

#### 3.1. Basic Principles of Radio Frequency Identification

Typical wireless communication processing architectures include a baseband digital part, digital-to-analog conversion, filters, an IQ modulator, HPAs, and antennas, as shown in the bottom left part of Figure 2. RF features are produced when a signal passes through nonlinear modules. Actual stable, unchanging, subtle hardware impairments are features that we want to acquire [26]. The offset error of an analog-to-digital converter (ADC) is the difference between the center of the least significant bit (LSB) and the ideal ADC with the same bits. We always treat converter quantization interval as LSB. We measure the first and last threshold of the converter to determine the precise location of the ideal center. The *LSB* is defined as

$$V_{LSB} = \frac{V_{FSR}}{2^{N_{bits}}} \tag{1}$$

where  $V_{FSR}$  is the full-scale range of the ADC.  $N_{bits}$  are the ADC bits that represent the precision of ADC, and  $2^{N_{bits}}$  denotes the number of voltage intervals. We can rewrite the error function with  $V$  as

$$E_{offset} = 2^{N_{bits}} \frac{V_{Error}}{V_{FSR}} \tag{2}$$

we can define a normalized unit's linearity errors  $G_{ADC}$  as

$$G_{ADC} = \frac{E_{offset}}{V_{FSR}} \tag{3}$$

The DC component of analog IQ signals is the main source of carrier leakage. As shown in Figure 3, IQ mismatch contains offset, imbalance, and error.  $I_{offset}$  and  $Q_{offset}$  represent the relative value of the respective signal amplitudes. All those impairments form partial unique fingerprint features. We can assess carrier rejection through factor  $\alpha$

$$\alpha = 20lg(\sqrt{I_{offset}^2 + Q_{offset}^2}) \tag{4}$$

we can evaluate practical I/Q imbalance (shown in Figure 4) through the following equation.

$$G_{IQ} = \sqrt{\frac{1 + \alpha^2 - 2\alpha\cos(\epsilon)}{1 + \alpha^2 + 2\alpha\cos(\epsilon)}} \tag{5}$$

The radio frequency filter is the key module in communication systems, and is mainly responsible for the suppression of noise and illegal signals outside the working frequency band. However, limited by material characteristics and implementation, high-frequency filters often cannot achieve ideal performance.  $G_{Filter}$  is always utilized to denote filter nonlinearity such as Q value, insertion loss, and phase jitter. The power amplifier (PA) is the last module before transmission. Although digital predistortion (DPD) can be utilized to compensate for nonlinear characteristics of PA, harmonic and intermodulation distortion still occur in a high-saturation state. Inevitable distortion caused by PA can be denoted by  $G_{Amp}$ .

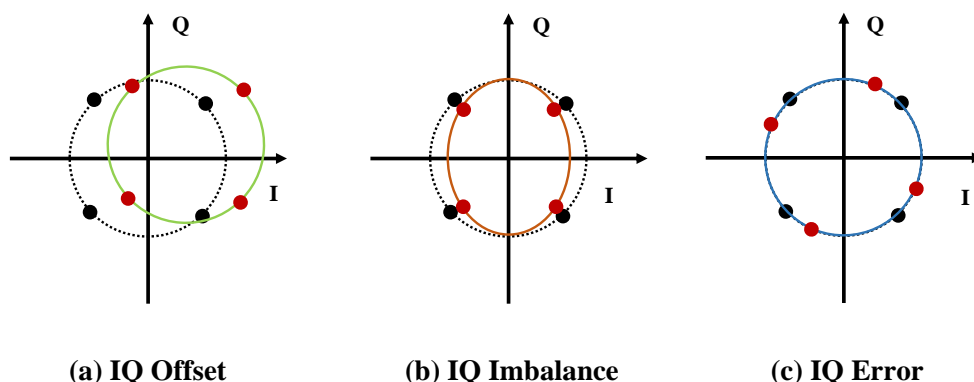


**Figure 3.** Composition of IQ mismatch. (a) IQ offset causes carrier leakage, which is very obvious from a spectral point of view. (b) IQ imbalance mainly refers to the difference in analog I and Q signal amplitudes of digital-to-analog convert (DAC) output, and the gain imbalance of an analog IQ modulator. (c) IQ error is the bad orthogonality between two LO signals in the analog IQ modulator.

In order to verify and evaluate whether the nonlinearity of the different modules above forms a radio fingerprint, we collected different mobile device signals in a routine environment on the basis of the system-processing flow in Figure 2. The collected signal is represented by

$$x_i = G_{IQ}G_{ADC}G_{Filter}G_{Amp}s_i = Gs \tag{6}$$

where  $s_i$  is the original binary information, and  $G$  is the nonlinear fingerprint. We carried out preliminary demodulation on the basis of collected samples. Figure 4 shows that two different devices indicated relatively obvious differences from the perspective of the constellation. Therefore, the radio fingerprint based on hardware impairment was stable while exiting, and could be further mined and processed. So, a deep-learning framework is the most suitable solution due to its massive nonlinear layer-to-layer neurons.

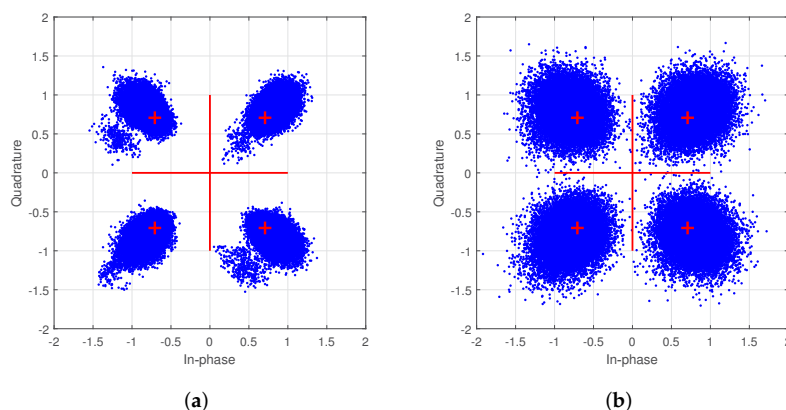


**Figure 4.** Constellation corresponding to two different real mobile devices' SRS frame in the same environment. (a) Nonlinear characteristics of device1 in constellation. (b) Nonlinear characteristics of device2 in constellation.

### 3.2. Novel Architecture Illustration of Semisupervised Learning Model

Supervised learning requires massive numbers of labeled training samples to guarantee the promised performance [30]. Semisupervised learning shown in Figure 5b, i.e., joint learning from labeled and unlabeled samples, is an active research topic due to its key role on relaxing human supervision. Despite the strong performance of pseudolabel methods, there is still a main drawback: if pseudolabels are inaccurate, the student network must learn from an inaccurate parameter [36]. The student network may not achieve significantly better performance than that of the pretrained teacher network, which is called confirmation bias. To solve the above problems, the authors systematically designed a solution framework to reduce false label learning bias [34]. In this framework, we designed such a mechanism where the teacher network could obtain information from student predictions, which is used to further correct soft label decisions for unlabeled data. To elaborate the mutual learning process between the two networks, we rewrote the cross-entropy loss function on the basis of the student network:

$$w_s^{ssl} = \arg \min_{w_s} \mathbb{E}_{x_u} [\mathcal{C}(T(x_u; w_t), S(x_u; w_s))] \quad (7)$$

where  $w_s$  and  $w_t$  represent the weight parameters of the teacher and student networks.  $(x_u, x_l, y_l)$  refer to the batch of training data that consist of  $x_u$ ,  $x_l$  and corresponding labels  $y_l$ , respectively.  $T(), S()$  denotes the soft prediction decisions of input data. We used  $\mathcal{C}()$  to describe the cross-entropy between different distributions. Furthermore, we used  $\mathbb{E}_{x_l, y_l} [\mathcal{C}(y_l, S(x_l; w_s^{ssl}))]$  to represent student loss on labeled samples  $L_l(w_s^{ssl})$ . The minimal value of student network loss function is the optimal solution in the network training process; the optimizing problem can be described as

$$\min_{w_t} L_l(w_s^{ssl}(w_t)) \quad (8)$$

where  $w_s^{ssl}(w_t) = \arg \min_{w_s} L_u(w_t, w_s)$ , and due to the mutual promotion learning of two networks, accurate gradient descent leads to a huge amount of computation. The idea is to approximate  $w_s^{ssl}(w_t)$  by using only a single training step to completely replace the inner optimization by training until convergence. Related techniques are used in metalearning, gradient-based hyperparameter tuning, and unrolled generative adversarial networks. Therefore, the approximate expansion is used to retain the maximal term and can be described as

$$w_s^{ssl}(w_t) \approx w_s - \eta_s \cdot \nabla_{w_s} L_u(w_t, w_s) \quad (9)$$

Then, we can substitute (9) into (8) to obtain

$$\min_{w_t} L_l(w_s - \eta_s \cdot \nabla_{w_s} L_u(w_t, w_s)) \quad (10)$$

In order to solve the optimization problem above, we need to minimize the student network loss function by adjusting the weight of the teacher network. We can obtain the derivatives by chain rule

$$\begin{aligned} \frac{\partial L_l(w_s^{ssl}(w_t))}{\partial w_t} &= \frac{\partial}{\partial w_t} \mathcal{C} \left( y_l, \underbrace{S(x_l; \mathbb{E}_{\hat{y}_u \sim T(x_u; w_t)} [w_s - \eta_s \nabla_{\eta_s} \mathcal{C}(\hat{y}_u, S(x_u; w_s))])}_{\text{student predication}} \right) \\ &= \frac{\partial}{\partial w_T} \mathcal{C}(y_l, S(x_l; \bar{w}'_s)) \\ &= \underbrace{\frac{\partial \mathcal{C}(y_l, S(x_l; \bar{w}'_s))}{\partial w_s}}_{\text{Part I}} \bigg|_{w_s = \bar{w}'_s} \cdot \underbrace{\frac{\partial \bar{w}'_s}{\partial w_t}}_{\text{Part II}} \end{aligned} \quad (11)$$

where,

$$\bar{w}'_s = \mathbb{E}_{\hat{y}_u \sim T(x_u; w_T)} [w_s - \eta_s \nabla_{\eta_s} \mathcal{C}(\hat{y}_u, S(x_u; w_s))] \quad (12)$$

As shown in (11), the Part I factor can be calculated by backpropagation. Then, we can rewrite Part II as following

$$\begin{aligned} \frac{\partial \bar{w}'_s}{\partial w_t} &= \frac{\partial}{\partial w_t} \mathbb{E}_{\hat{y}_u \sim T(x_u; w_t)} [w_s - \eta_s \nabla_{\eta_s} \mathcal{C}(\hat{y}_u, S(x_u; w_s))] \\ &= \frac{\partial}{\partial w_t} \mathbb{E}_{\hat{y}_u \sim T(x_u; w_t)} \left[ w_s - \eta_s \cdot \left( \frac{\partial \mathcal{C}(\hat{y}_u, S(x_u; w_s))}{\partial w_s} \right)^T \right] \end{aligned} \quad (13)$$

where  $w_s$  is independent with  $w_t$ , and we can leave the first part out of subsequent derivations. Furthermore, we can obtain the simplified expression as

$$\begin{aligned} \frac{\partial \bar{w}'_s}{\partial w_t} &= -\eta_s \cdot \frac{\partial}{\partial w_t} \mathbb{E}_{\hat{y}_u \sim T(x_u; w_t)} \left[ \left( \frac{\partial \mathcal{C}(\hat{y}_u, S(x_u; w_s))}{\partial w_s} \right)^T \right] \\ &= -\eta_s \cdot \frac{\partial}{\partial w_t} \mathbb{E}_{\hat{y}_u \sim T(x_u; \theta_T)} [g_s(\hat{y}_u)] \end{aligned} \quad (14)$$

where

$$g_s(\hat{y}_u) = \left( \frac{\partial \mathcal{C}(\hat{y}_u, S(x_u; w_s))}{\partial w_s} \right)^T \quad (15)$$

(15) shows that  $g_s(\hat{y}_u)$  has no dependency on  $w_t$ , except for via  $\hat{y}_u$ . So, the REINFORCE equation [34] was applied to obtain

$$\begin{aligned} \frac{\partial \bar{w}'_s}{\partial w_t} &= -\eta_s \cdot \frac{\partial}{\partial w_t} \mathbb{E}_{\hat{y}_u \sim T(x_u; w_t)} [g_s(\hat{y}_u)] \\ &= \eta_s \cdot \mathbb{E}_{\hat{y}_u \sim T(x_u; w_t)} \left[ g_s(\hat{y}_u) \cdot \underbrace{\frac{\partial \mathcal{C}(\hat{y}_u, T(x_u; w_t))}{\partial w_t}}_{\text{gradient of cross-entropy loss}} \right] \end{aligned} \quad (16)$$



Then, we can substitute (16) into (11) to acquire the final result:

$$\begin{aligned} \frac{\partial L_l(\bar{w}_s^{ssl}(w_t))}{\partial w_t} &= \underbrace{\frac{\partial \mathcal{C}(y_l, S(x_l; \bar{w}_s'))}{\partial w_s}}_{\text{PartI}} \Big|_{w_s=\bar{w}_s'} \cdot \underbrace{\frac{\partial \bar{w}_s'}{\partial w_t}}_{\text{PartII}} \\ &= \eta_s \cdot \frac{\partial \mathcal{C}(y_l, S(x_l; \bar{w}_s'))}{\partial w_s} \cdot \mathbb{E}_{\hat{y}_u \sim T(x_u; w_t)} \left[ g_s(\hat{y}_u) \cdot \frac{\partial \mathcal{C}(\hat{y}_u, T(x_u; w_t))}{\partial w_t} \right] \end{aligned} \tag{17}$$

For simplicity but without loss of generality, we can calculate the terms in (17) by utilizing Monte Carlo approximation with samples  $\hat{y}_u$ . Furthermore, we can approximate  $\bar{w}_s'$  by updating the student parameter on unlabeled samples through (12). With those approximations, final gradient  $\nabla_{w_t} L_l$  can be calculated by

$$\begin{aligned} \nabla_{w_t} L_l &= \eta_s \cdot \underbrace{\frac{\partial \mathcal{C}(y_l, S(x_l; w_s'))}{\partial w_s}}_{\text{labeled+student network}} \cdot \left( \underbrace{\frac{\partial \mathcal{C}(\hat{y}_u, S(x_u; w_s))}{\partial w_s}}_{\text{unlabeled+student network}} \Big|_{w_s=w_t} \right)^T \cdot \underbrace{\frac{\partial \mathcal{C}(\hat{y}_u, T(x_u; w_t))}{\partial w_t}}_{\text{unlabeled+teacher network}} \\ &= \eta_s \cdot \nabla_{w_s'} \mathcal{C}(y_l, S(x_l; w_s'))^T \cdot \nabla_{w_s} \mathcal{C}(\hat{y}_u, S(x_u; w_s)) \cdot \nabla_{w_t} \mathcal{C}(\hat{y}_u, T(x_u; w_t)) \end{aligned} \tag{18}$$

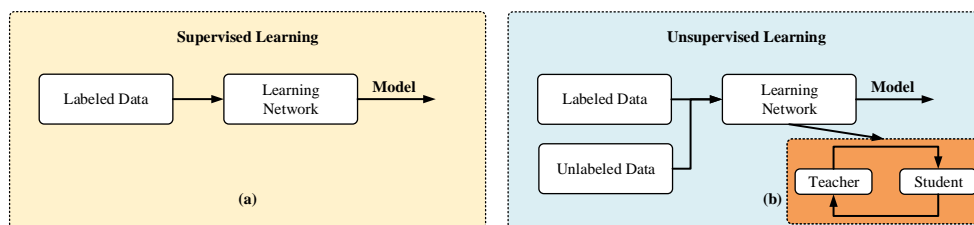


Figure 5. Main workflow of machine learning. (a) supervised learning. (b) semi-supervised learning.

On the other hand, the student’s training still relies on the objective in (7), except that the teacher parameter is not fixed anymore. The teacher’s optimization process involves changing. More interestingly, we also used SGD to update the weight, and the updated student’s parameter can be reused in the one-step approximation of the teacher’s objective. This design naturally gives rise to an alternating optimization procedure between student and teacher network updates, which can be denoted as

$$w_s' = w_s - \eta_s \cdot \nabla_{w_s} L_u(w_t, w_s) \tag{19}$$

$$w_t' = w_t - \eta_t \cdot \nabla_{w_t} L_l(w_s') \tag{20}$$

As shown in Figure 6, we constructed the one-dimensional RFIResNet by ID and conv blocks. We used two convolutional layers and an additional add module to form ID blocks. For conv blocks, there exists a dimensional transformation to realize vector length matching. First, the convolutional operation of the input signal is realized by 64 linear filters with a size of  $7 \times 1$ . All those kernels were designed to obtain characteristic information at different time scales. ReLu activation functions reduce the general gradient vanishing [30]. Furthermore, the proposed RFIResNet contains 42 layers to learn RF characteristics, and the total number of parameters was 11,304,907, which approximately equals to that in the original ResNet18. Lastly, we utilized a full connection layer and softmax function to realize dimension reducing and probability mapping. Cross entropy is used to guide the learning and convergence of the network model [37]. Furthermore, our proposed semisupervised learning framework with meta pseudo labels is shown as Algorithm 1.

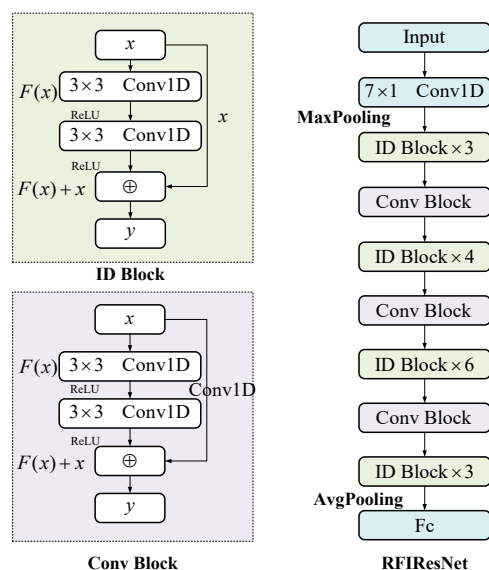


Figure 6. Illustration of one-dimensional RFIResNet architecture used in this paper.

#### Algorithm 1 RFISSL Algorithm

**Input:** Labeled data and label  $(x_l, y_l)$ , Unlabeled data  $(x_u)$

**Output:** Student network weights  $w_s^{(N)}$

- 1: Initializing network weight  $w_t^{(0)}, w_s^{(0)}$ .
- 2: **for**  $n = 0$  to  $N - 1$  **do**
- 3: Get pseudolabel  $\hat{y}_u$  through calculating probability  $P(\cdot | x_u; w_t)$
- 4: Update  $w_s$  by pseudolabel  $\hat{y}_u$ , where  $\eta_s$  denotes the adjustment factor, and  $\mathcal{C}$  denotes cross-entropy:  $w_s^{(n+1)} = w_s^{(n)} - \eta_s \nabla_{w_s} \mathcal{C}(\hat{y}_u, S(x_u; w_s^{(n)}))$
- 5: Compute the teacher's weight coefficient  $h$ :  $h = \eta_s ((\eta_s \nabla_{w_s} \mathcal{C}(y_l, S(x_u; w_s^{(n+1)})))^T \cdot \eta_s \nabla_{w_s} \mathcal{C}(\hat{y}_u, S(x_u; w_s^{(n)})))$
- 6: Compute the teacher's gradient  $g_t^{(n)}$ :  $g_t^{(n)} = h \cdot \nabla_{w_t} \mathcal{C}(\hat{y}_u, T(x_u; w_t^{(n)}))$
- 7: Calculating the teacher's gradient  $g_{t, supervised}^{(n)}$  on the basis of labeled data:  $g_{t, supervised}^{(n)} = \nabla_{w_t} \mathcal{C}(\hat{y}_l, T(x_l; w_t^{(n)}))$
- 8: Update teacher network's weight:  $w_t^{n+1} = w_t^n - \eta_t \cdot (g_t^{(n)} + g_{t, supervised}^{(n)})$
- 9: **end for**
- 10: **return:**  $w_s^{(N)}$

## 4. Transmission Performance Analysis of RFI-Aided URLLCs with Massive MIMO

### 4.1. Error Probability Bound for Random Channels

In this section, we consider a simple case where the channel is assumed to have Gaussian distribution. Then, we establish an evaluation framework of URLLCs error probability with finite block-length uplink transmission. Due to the symmetry of uplink and downlink transmissions, our paper discusses uplink transmission performance. For simplicity but without loss of generality, the performance downlink is similar to uplink transmission. Furthermore, we involve massive MIMO into the system to assess the suitability for short-packet URLLCs. A typical channel model can be expressed as

$$y(m) = \mathbf{h}G_s(m) + z(m) = \mathbf{h}x(m) + z(m), \quad m = 1, \dots, n \quad (21)$$

where  $x(m) \in \mathbb{C}$  and  $y(m) \in \mathbb{C}$  represent the input and output of channel, respectively.  $\mathbf{h}$  denotes the channel gain, which is assumed to be a quasistatic variable during packet transmission.  $z(m)$  is a sample of additive Gaussian noise  $\mathcal{CN}(0, \sigma^2)$  that satisfies the

independent and identically distributed (i.i.d) property. Then, we can obtain the estimated  $\hat{x}$  by

$$\hat{x} = \arg \min_{\tilde{x} \in \mathcal{C}} \|y - \hat{h}\tilde{x}\|^2 \tag{22}$$

where  $\tilde{x}$  denotes the predefined codeword, and  $\hat{h}$  is the estimation of  $h$  at the receiver. Equation (22) shows that it is a classical decoder to estimate an original signal by minimizing Euclidean distance [38]. Then, we can obtain the error probability bound by

$$P_{Error} = \mathbb{P}[\hat{x} \neq x] \leq \mathbb{P}\left[\sum_{m=1}^n \gamma_s(x(m), y(m)) + \log(u) \leq \log(k-1)\right] \tag{23}$$

where  $u$  is a uniformly distributed random variable, and  $\gamma_s$  represents information density, which is defined as follows [16]:

$$\gamma_s(x(m), y(m)) = -s \left| y(m) - \hat{h}x(m) \right|^2 + \frac{s|y(m)|^2}{1 + s\rho|\hat{h}|^2} + \log\left(1 + s\rho|\hat{h}|^2\right) \tag{24}$$

where  $\rho$  is considered to be the transmission power of an average packet. Due to random channel gain  $h \in \mathbb{C}$  satisfying an arbitrary distribution, we can rewrite (23) as

$$P_{Error} = \mathbb{P}[\hat{x} \neq x] \leq \mathbb{E}_{h, \hat{h}} \left[ \mathbb{P}\left[\sum_{m=1}^n \gamma_s(x(m), y(m)) \leq \log \frac{k-1}{u} \mid h, \hat{h}\right] \right] \tag{25}$$

where the average is taken over the random distribution of  $h$ . For general applications of infinite block-length transmission, Shannon capacity is the upper bound of the whole total system [13]. Furthermore, the error probability of URLLCs can be defined as the probability that the empirical average of generalized information density  $\gamma_s$  described in (23) is smaller than chosen rate  $R$ . As introduced in (25), an accurate closed-form mathematical solution can only be calculated by numerical simulations. Normal approximation (NA) is an efficient method to solve the huge calculation-consuming problem by utilizing the Berry–Esseen central limit theorem. On this basis, we can rewrite (25) as

$$\mathbb{P}\left[\sum_{m=1}^n \gamma_s(x(m), y(m)) \leq \log \frac{k-1}{u}\right] = Q\left(\frac{nI_s - \log(k-1)}{\sqrt{n}J_s}\right) + o\left(\frac{1}{\sqrt{n}}\right) \tag{26}$$

where  $I_s$  denotes mutual information, and  $Q$  represents Gaussian  $Q$  function.  $J_s$  defines the variance in information density. However, the approximation accuracy of NA is not robust for URLLC applications. Saddle-point approximation is a novel method to solve the huge calculation-consuming problem [39]. By using saddle-point approximation, we can obtain new representation of error probability.

$$\mathbb{P}\left[\sum_{m=1}^n I_s(x(m), y(m)) \leq \log \frac{e^{nR}-1}{u}\right] = e^{n[\kappa(\zeta) + \zeta R]} \left[ \Theta_{n, \zeta}(\zeta) + \Theta_{n, \zeta}(1 - \zeta) + o\left(\frac{1}{\sqrt{n}}\right) \right] \tag{27}$$

where

$$\Theta_{n, \zeta}(u) \triangleq e^{n\frac{u^2}{2}\kappa''(\zeta)} Q\left(u\sqrt{n\kappa''(\zeta)}\right) \tag{28}$$

where  $\mathcal{O}\left(\frac{1}{\sqrt{n}}\right)$  denotes residual error. The cumulant-generating function of saddle-point approximation can be described as  $-\kappa(\zeta)$ . We assumed that  $k = e^{nR}$  for  $R > 0$ . Furthermore,

the right-hand side part of (27) corresponds to Gallager’s error exponent for the wrong decoding application.

$$P_{error} = \begin{cases} e^{n[\log \mathbb{E}[e^{-\gamma s(x(m),y(m))}] + R]} \left[ \tilde{\Theta}_n(1, 1) + \tilde{\Theta}_n(0, -1) + \mathcal{O}\left(\frac{1}{\sqrt{n}}\right) \right] & \zeta > 1, R < R_{critical} \\ 1 - e^{n[\kappa(\zeta) + \zeta R]} \left[ \Theta_{n,\zeta}(-\zeta) - \Theta_{n,\zeta}(1 - \zeta) + o\left(\frac{1}{\sqrt{n}}\right) \right], & \zeta < 0, R > I_s \end{cases} \quad (29)$$

where

$$\tilde{\Theta}_n(a_1, a_2) = e^{na_1 \left[ R_{critical} - R + \frac{\kappa''(1)}{2} \right]} \times Q \left( a_1 \sqrt{n\kappa''(1)} + a_2 \frac{n(R_{critical} - R)}{\sqrt{n\kappa''(1)}} \right) \quad (30)$$

and  $R_{critical} = -\kappa'(1)$  represents the critical system rate. The subexponential factor is estimated by saddle-point approximation to acquire accurate error probability [16]. From (29), we can find that separating Gallager’s error exponent is the main process of saddle-point approximation. Then, the Berry–Esseen central-limit theorem is applied to calculate factors before the exponential term.  $P_{error}$  represents the error probability for finite block-length transmission.

#### 4.2. Reliability Analysis for RFI-Aided URLLCs

In this section, a single cell where the BS is equipped with  $M$  antennas serving two single-antenna smart devices is considered. A Rayleigh fading channel is involved to characterize the actual channel. We used  $\mathbf{h}$  to denote the channel vector between BS and smart device. Wireless transmission relied on pilot  $\ell_{pilot} \in \mathbb{C}$ , and channel correlation directly affects BS performance. We used orthogonal pilot sequences to reduce mutual interference between different devices as much as possible. That means that  $\ell_{pilot}$  satisfies  $\ell_{pilot}^i \times \ell_{pilot}^j = 0$ , and the element pilot sequence is scaled by transmission power  $\sqrt{\rho_{ul}}$ . At the receiver side, received pilot signal  $y_{pilot} \in \mathbb{C}$  can be expressed as

$$y_{pilot} = \sqrt{\rho_{ul}} h_i \ell_i^H + \sqrt{\rho_{ul}} h_j \ell_j^H + z_{pilot} \quad (31)$$

where  $z_{pilot} \in \mathbb{C}$  denotes the additive Gaussian noise with distribution  $\mathcal{CN}(0, \sigma^2)$ .  $h_i$  is the fading channel vector. Furthermore, for accurately recovering the original signal on the receiving side, it is necessary to accurately estimate channel vector  $h$ . Minimal mean squared error (MMSE) is a remarkable method to estimate  $h$  by

$$\hat{h}_i = \sqrt{\rho_{ul}} n_p \mathbf{R}_i \mathbf{W}_i^{-1} (y_{pilot} \ell_i) \quad (32)$$

where

$$\mathbf{W}_i = \sum_{l=1}^K \rho_{ul} \mathbf{R}_l \ell_l^H \ell_l + \sigma^2 \mathbf{I}_M \quad (33)$$

and  $K = 2$  denotes two different smart devices.  $\mathbf{R}$  is the correlation matrix of spatial channel, which indicates the quality of different channels. It is clear from (33) that, if pilot sequences are orthogonal, i.e.,  $\ell_j^H \ell_i = 0$ , there is no interference in channel estimation. Furthermore, if underlying channels  $h_1$  and  $h_2$  are independent from each other, this means that  $h_1 h_2^H = 0$ . Then, channel gain is independent scaling factor  $r_i$ , which is the diagonal element of  $\mathbf{R} = \beta_i \mathbf{I}_M$ . Uplink transmission can be described as

$$y_{ul}(m) = \sum_{i=1}^K h_i x_{ul,i}(m) + z_{ul} \quad (34)$$

where  $x(m)$  denotes the original signal that is transmitted by the  $i$ -th smart device with average power  $\rho_{ul}$ .  $z_{ul}$  is the Gaussian additive noise satisfying i.i.d properties. We can

estimate  $\hat{x}_{ul}$  through estimation-combined channel vector channel  $V_i$ , which can be obtained by computational algorithm MMSE in (35).

$$V_i = \left( \sum_{i=1}^K \hat{h}_i \hat{h}_i^H + Z \right)^{-1} \hat{h}_i \tag{35}$$

where  $Z = \sum_{i=1}^k \Phi_i + \frac{\sigma_{ul}^2}{\rho_{ul}} \mathbf{I}_M$  denote mutual interference between different devices. Furthermore, we can obtain signal  $x_{ul,i}(m)$  by utilizing combined vector  $V_i$  as follows:

$$r_{ul,i}^{ul}[k] = V_i^H \sum_{i=1}^K h_i x_{ul,i}(m) + V_i^H z_{ul} \tag{36}$$

Similar to (21), (36) has the same form. Assuming that BSs achieve a perfect estimation of channel can obtain the final codeword by

$$\hat{x}_{ul,i} = \arg \min_{\tilde{x}_{ul,i} \in \mathcal{C}_{ul}} \left\| r_{ul,i} - \left( V_i^H \hat{h}_i \right) \tilde{x}_{ul,i} \right\|^2 \tag{37}$$

To obtain the average error probability of uplink transmission, we refer to the calculation process of (23). A simplified expression can be written as

$$P_{ul,i} \leq \mathbb{E} \left[ \mathbb{P} \left[ \sum_{i=1}^{n_{ul}} \gamma_s(r_{ul,i}(m), x_{ul,i}(m)) \leq \log \frac{k-1}{u} \mid V_i^H h_i, V_i^H \hat{h}_i, \sigma^2 \right] \right] \tag{38}$$

where  $n_{ul}$  represents the number of uplink transmissions. The saddle-point approximation described in Section 4.1 can be used to efficiently and accurately calculate probability in (38). In summary, since short-packet transmission is different from traditional Shannon capacity theory, we utilized saddle-point approximation to reduce complexity and obtain a closed-form solution that is introduced in detail in the next section.

### 5. Results and Discussion

In this section, we provide extensive experiments on large-scale LTE datasets for radio frequency identification with an SSL model. Simulation results of RFI-aided URLLCs uplink transmission are provided to validate the error probability and availability of the network system.

#### 5.1. RFISL Experiments Setup and Performance

To comprehensively evaluate the identification performance of our proposed RFISL model, we established a practical LTE scenario dataset by collecting raw time-signal data from the 30 smart devices listed in Table 1. For simplicity but without loss of generality, those devices represent a typical application in an industrial scenario. In our system configuration, two different sounding reference signal (SRS) symbols were located in symbols 4 and 11 of a regular frame. Through the long-term static acquisition of all devices, we obtained nearly 40,000 frames of data for each mobile phone, with a total dataset size of about 50 GB, which could be used to evaluate the ability of various complex networks to extract device fingerprint features. After obtaining a signal, we conducted some preprocessing operations, mainly including the normalization and dimension transformation of the signal [30]. On this basis, the training and testing samples were established in a raw series.

During the experimental process, we only selected few labeled samples, and the rest of the samples were selected to be unlabeled data to assist in the mutual learning of the two RFIResNets. We configured a 42 layer one-dimensional network with a ReLU activation function to construct the RFISL framework. We used  $(x_l, y_l)$  to represent the labeled data, where  $x_l$  denotes collected time signals, and  $y_l$  denotes the device label listed in Table 1. Unlabeled data  $(x_{ul},)$  only contain time signals without a device label.

The key mechanism of RFISSL is that the teacher network learns the weight feedback of students under pseudolabels to further improve its performance and generate more accurate soft labels.

**Table 1.** List of smart devices in experiments.

Group	Phone	Number of UE	Label
1	Iphone6s	5	1–5
2	Xaiomi6	5	6–10
3	Meizux8	5	11–15
4	Honor10	5	16–20
5	Huaweip9	5	21–25
6	Oppor11	5	26–30

As shown in Figure 7a, various percentages of labeled data were examined by RFISSL and compared with SL models such as ResNet18-1D, VGG16-1D, and AlexNet under different training samples [40]. This chart shows that RFISSL achieved almost 0.1 identification error with only 1% of labeled training samples, matching fully supervised learning with 100% of labeled instances. Lower error can also be exploited by RFISSL with an increase in the percentage of labeled instances. When trained with 4500 labeled samples, RFISSL achieved almost  $10^{-5}$  error. We also evaluated several SL models and found that VGG16-1D and ResNet18-1D, which were trained with 4500 labeled samples, only achieved performance that RFISSL could achieve only with 10% labeled samples (total slicenum equal to 2700). Furthermore, we transformed our one-dimensional signals into time–frequency data by short-time Fourier transform (STFT). Then, we analyzed identification performance under AlexNet. The result in Figure 7a shows that AlexNet achieved better performance than that of VGG16-1D due to its lager network parameters. These excellent properties confirmed the benefit of efficient student and teacher feedback learning. In the process of network training, two networks need to continuously learn from each other. Due to the existence of unlabeled samples, the training process has a huge cost, but the testing of network model needed about 0.52 ms on the server. This satisfies the requirement of practical URLLCs. Figure 7a shows that consistent gains confirmed the benefit of internal distribution characteristic deviation of device features.

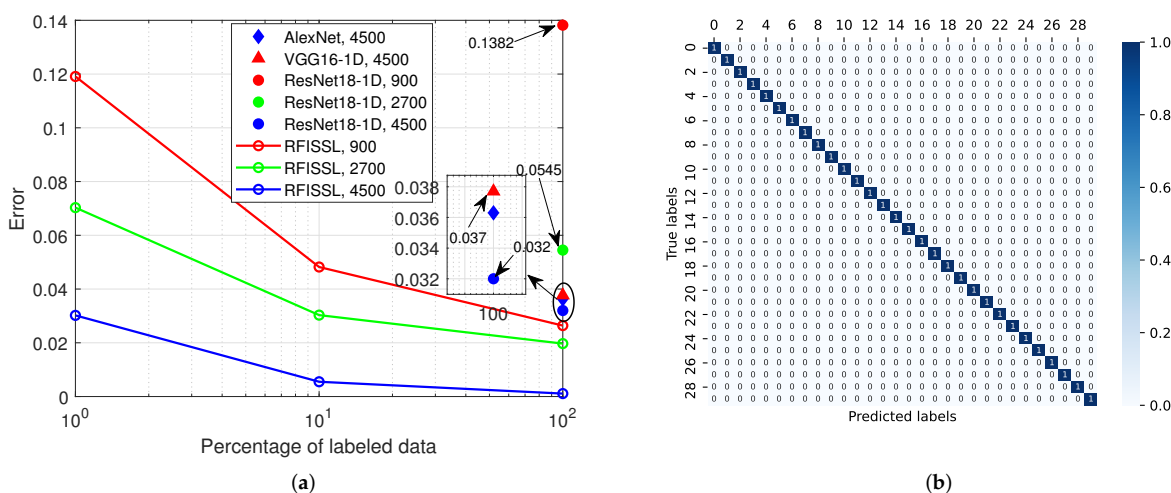


**Figure 7.** RFISSL performance. (a) Identification accuracy of RFISSL under different percentages of labeled data. Both models tested with LTE dataset. (b) Confusion matrices for RFISSL model trained without augmentation when labeled training samples equals to 4500.

Figure 7b again confirms that our proposed RFISSL could truly realize almost  $10^{-5}$  RF identification error of a large-scale smart device with 4500 training samples. Our RFI error

probability  $P_{RFI}$  could thus be reduced by utilizing a meta pseudo label. The deep learning model could be deployed at resource-constrained computing units by using structured pruning to render the model sparse [41]. Furthermore, the total error probability of RFI-aided URLLCs is discussed in Section 5.2.

5.2. Average Error Probability Bound of Short Packet URLLCs

For the simulation of proposed RFI-aided URLLCs with short packet, we drew on potential deployment schemes for URLLCs from existing works [28] to establish typical application scenarios. For simplicity but without loss of generality, a 2D scenario is considered in Figure 8. The BS located at (0, 100) and two smart devices were involved. In our simulation setup, Device 2 was located at fixed position (57.7, 0) and Device 1 could move along the  $x$  axis. To acquire a general analytical framework of the error probability bound, an additive Gaussian channel and Device 2 were assumed in first stage. Our system was configured with 20 MHz bandwidth. The error probability definition in (23) shows that, if the BS acquires perfect channel state information, then  $P_{Error}$  converges to the outage probability, which can be defined as

$$P_{Error} = \mathbb{P} \left[ \log \left( 1 + \frac{\rho h^2}{\sigma^2} \right) < R \right] \tag{39}$$

where  $h$  denotes the channel gain, and  $R$  represents the upper bound of information rates. Lastly, for the joint RFI-aided URLLCs framework, we could obtain total error probability by

$$P = 1 - P_{RFI} (1 - \mathbb{P} \left[ \log \left( 1 + \frac{\rho h^2}{\sigma^2} \right) < R \right]) \tag{40}$$

where  $P_{RFI}$  represents error detection probability, and  $P$  denotes total system error probability. RFI accuracy performance impacts general system reliability. We achieved physical access without any additional overload, and all those time–frequency resources could be utilized to transmit useful information.

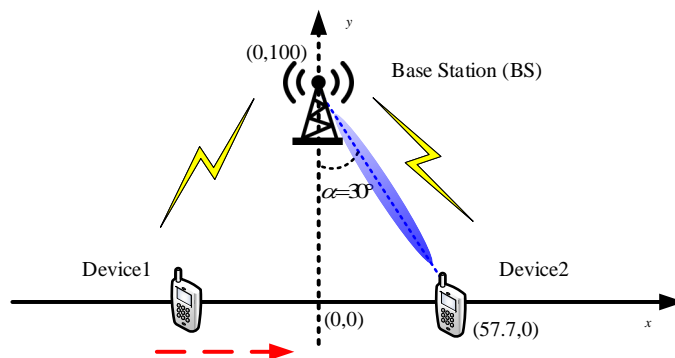
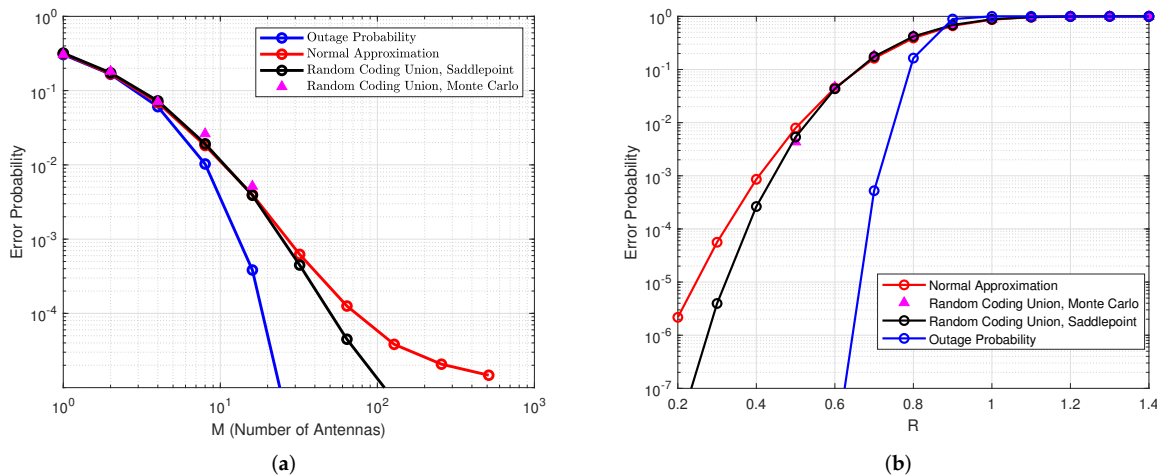


Figure 8. Simulation scenario with BS located at (0, 100) and assisted by massive MIMO serving two different intelligent devices.

As shown in Figure 9a, theoretical outage probability and approximation methods were compared. We assumed that they all had the same received SNR. Results demonstrate that the saddle-point approximation matched well with Monte Carlo testing. With the increase in number of antennas  $M$ , there was a gradual difference in those methods due to the estimation error except saddle-point approximation. Figure 9b shows the relationship between  $R$  and error probability. Specifically, a fixed number of antennas  $M = 128$  is considered. Only the saddle-point method was an exact actual random coding union (RCU) bound. In summary, outage probability and normal approximation do not always provide good estimations of the error probability achievable in URLLCs with massive MIMO over quasistatic channels.



**Figure 9.** Average error probability of uplink transmission with massive MIMO. Single UE is assumed to connect with BS and  $\mathbf{h} \sim \mathcal{CN}(\mathbf{0}_M, \beta \mathbf{I}_M)$ . (a) Error probability under different numbers of antennas and approximation methods with  $R = 0.6$ . (b) Performance of URLLCs with different  $R$ , where  $M = 256$ .

### 5.3. Uplink Transmission Performance of Multiple Devices with Massive MIMO

Impact spatial correlation  $Corr$  and number of antennas  $M$  are investigated here. As shown in Figure 8, we assumed that there existed two smart devices connected to a single BS at (0, 100). A horizontal uniform linear array (ULA) was established to achieve massive MIMO. Furthermore, we assumed that channel scatters were randomly distributed in the path of BS and devices [42]. Then, we could describe the angular distribution by  $(\theta_i \pm \delta)$ , where  $\theta_i$  denotes the angle of arrival (AoA) of the  $i$ -th device, and  $\delta$  is the scatter spread. The large-scale fading coefficient was modeled in [43]. The transmission power of uplink was assumed to be 10 mW, and the noise level of receiver to be about  $-100$  dBm. A typical uplink transmission contains about 100 bits of information. In Figure 10, the impact of antenna number  $M$  with different positions is investigated. Results demonstrates that error probability sharply deteriorated with the shortening of the distance between two devices, and a larger number of antennas provide better system performance.

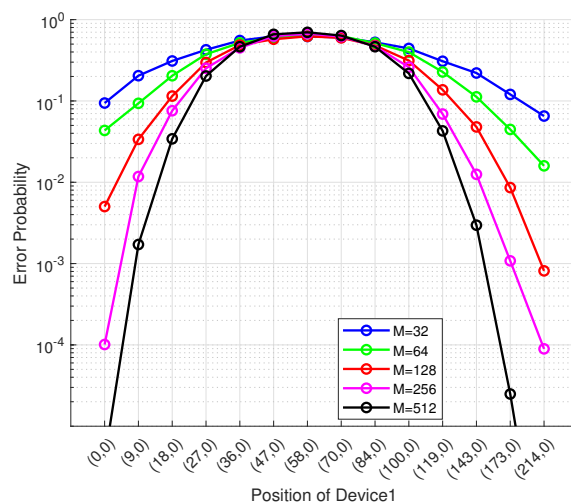


**Figure 10.** Uplink transmission error probability against different positions of Device 1 with  $n = 100$  and fixed transmission power. Device 2 located at (57.7, 0).

In order to validate the asymptotic analysis of channel correlation, we numerically evaluated the uplink transmission error probability when two devices transmit at the same



power and pilot sequence. Furthermore, we assumed that the devices were located at (0, 0), and their channel correlation could be designed for evaluating the significant impact on error probability. As shown in Figure 11a, average error probability as a function of  $M$  with different levels of channel correlation is investigated. These results demonstrate that channel correlation can directly influence system error probability. However, with the increase in  $M$ , system performance can be greatly improved due to the promotion of spatial freedom.

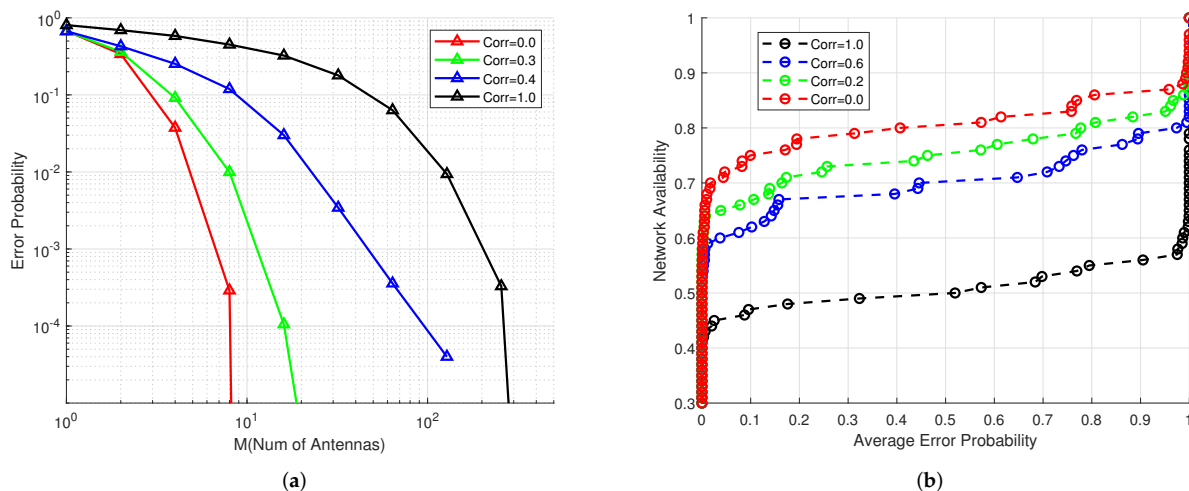


**Figure 11.** Performance of URLLC uplink transmission. (a) Error probability against number of antennas  $M$  with different channel correlation levels. (b) Network availability against average error probability with different channel correlation levels.

To gain more insight into the proposed RFI-aided URLLCs network from different perspectives, we defined network availability  $P_{Ava} = \mathbb{P}(P \leq P_{Ave})$  to measure the probability that satisfied the condition where  $P$  is calculated by uniformly distributing in the serving area of BS. As shown in Figure 11b,  $P_{Ava}$  increased with the increase in average error probability  $P_{Ave}$ . Interference caused by channel correlation significantly reduced network availability, irrespective of the processing scheme. There existed a very rapid upward trend when  $P_{Ave}$  was equal to 0 or 1 because, when uniformly distributing the devices, it is almost impossible that they always be located at excellent or low-SNR serving areas of BS. Therefore, carefully deploying smart devices guarantees balancing transmission efficiency and robustness in practical URLLCs systems.

### 6. Conclusions

In this paper, we first proposed an RFI-aided URLLCs system with massive MIMO that aims to improve transmission efficiency and access robustness with low cost and computational complexity. To obtain a remarkable machine-learning-based model, we involved SSL with meta pseudo labels. We established a novel one-dimensional RFIResNet for smart devices’ physical-layer access. We experimentally validated the performance of RFISSL on the basis of practical LTE datasets, and results showed that identification error converged to  $10^{-5}$ , with samples equal to 4500. In the proposed short-packet URLLC network, in a typical industrial application, we formulated the general analytical framework of finite block-length uplink transmission, which is the downlink symmetry. Our proposed RFISSL model only needed about 0.52 ms to finish online physical-layer access with limited computing resources. This satisfies the requirement of practical URLLCs. Furthermore, we provided an evaluation of the error probability bound and network availability by utilizing saddle-point approximation. Lastly, numerical experiment results demonstrated that introducing RFI and massive MIMO into URLLCs is a promising technique to improve transmission efficiency and robustness.

**Author Contributions:** Conceptualization, T.Z., P.R. and D.X.; methodology, T.Z.; software, T.Z. and Z.R.; validation, T.Z.; formal analysis, T.Z. and Z.R.; investigation, T.Z. and Z.R.; resources, P.R. and D.X.; data curation, T.Z.; writing—original draft preparation, T.Z.; writing—review and editing, T.Z., P.R., Z.R. and D.X.; visualization, T.Z. and Z.R.; supervision, P.R. and D.X.; project administration, T.Z. and P.R.; funding acquisition, P.R. All authors have read and agreed to the published version of the manuscript.

**Funding:** The work was completed with the financial support of National Natural Science Foundation of China under grant no. 62071373 and the Innovation Talents Promotion Program of Shaanxi Province under Grant No. 2021TD-08.

**Institutional Review Board Statement:** not applicable.

**Informed Consent Statement:** not applicable.

**Data Availability Statement:** The datasets in this paper can be downloaded from <https://github.com/ZhanyiRen/LTE-Datasets.git> (accessed on 15 March 2022).

**Conflicts of Interest:** the authors declare no conflict of interest.

## Abbreviations

The following abbreviations are used in this manuscript:

URLLCs	Ultrareliable and low-latency communications
TSN	Time-sensitive networking
5G	Fifth-generation
MIMO	Multi-input multioutput
RFI	Radio frequency identification
BSs	Base stations
UEs	User equipment
SSL	Semisupervised learning
IIoT	Intelligent Internet of Things
3GPP	3rd generation partnership project
I/Q	Inphase/quadrature
DCNNs	Deep convolutional networks
TDMA	Time division multiple access
ADC	Analog-to-digital converter
LSB	Least significant bit
NA	Normal approximation
MMSE	Minimal mean squared error
SRS	Sounding reference signal
RCU	Random coding union
ULA	Uniform linear array

## References

- Yeole, A.S.; Kalbande, D.R. Use of Internet of Things (IoT) in healthcare: A survey. In Proceedings of the ACM Symposium on Women in Research 2016, Indore, India, 21–22 March 2016; pp. 71–76.
- Colman-Meixner, C.; Khalili, H.; Antoniou, K.; Siddiqui, M.S.; Papageorgiou, A.; Albanese, A.; Cruschelli, P.; Carrozzo, G.; Vignaroli, L.; Ulisses, A.; et al. Deploying a novel 5G-enabled architecture on city infrastructure for ultra-high definition and immersive media production and broadcasting. *IEEE Trans. Broadcast.* **2019**, *65*, 392–403. [[CrossRef](#)]
- Shafi, M.; Molisch, A.F.; Smith, P.J.; Haustein, T.; Zhu, P.; De Silva, P.; Tufvesson, F.; Benjebbour, A.; Wunder, G. 5G: A tutorial overview of standards, trials, challenges, deployment, and practice. *IEEE J. Sel. Areas Commun.* **2017**, *35*, 1201–1221. [[CrossRef](#)]
- Letaief, K.B.; Shi, Y.; Lu, J.; Lu, J. Edge Artificial Intelligence for 6G: Vision, Enabling Technologies, and Applications. *IEEE J. Sel. Areas Commun.* **2021**, *40*, 5–36. [[CrossRef](#)]
- Centenaro, M.; Vangelista, L.; Saur, S. Analysis of 5G Radio Access Protocols for Uplink URLLC in a Connection-Less Mode. *IEEE Trans. Wirel. Commun.* **2020**, *19*, 3104–3117. [[CrossRef](#)]
- Alsenwi, M.; Tran, N.H.; Bennis, M.; Pandey, S.R.; Bairagi, A.K.; Hong, C.S. Intelligent Resource Slicing for eMBB and URLLC Coexistence in 5G and Beyond: A Deep Reinforcement Learning Based Approach. *IEEE Trans. Wirel. Commun.* **2021**, *20*, 4585–4600. [[CrossRef](#)]
- Chang, B.; Zhang, L.; Li, L.; Zhao, G.; Chen, Z. Optimizing resource allocation in URLLC for real-time wireless control systems. *IEEE Trans. Veh. Technol.* **2019**, *68*, 8916–8927. [[CrossRef](#)]

8. Xie, Y.; Ren, P.; Xu, D.; Li, Q. Optimizing Training and Transmission Overheads of URLLC in Industrial IoT Networks. In Proceedings of the 2020 IEEE Global Communications Conference Workshops (GLOBECOM Workshops), Taipei, China, 7–11 December 2020; pp. 1–6.
9. Ren, H.; Pan, C.; Wang, K.; Xu, W.; Elkashlan, M.; Nallanathan, A. Joint transmit power and placement optimization for URLLC-enabled UAV relay systems. *IEEE Trans. Veh. Technol.* **2020**, *69*, 8003–8007. [[CrossRef](#)]
10. Nayak, S.; Roy, S. Novel Markov Chain Based URLLC Link Adaptation Method for 5G Vehicular Networking. *IEEE Trans. Veh. Technol.* **2021**, *70*, 12302–12311. [[CrossRef](#)]
11. Ge, X. Ultra-reliable low-latency communications in autonomous vehicular networks. *IEEE Trans. Veh. Technol.* **2019**, *68*, 5005–5016. [[CrossRef](#)]
12. Ren, H.; Pan, C.; Deng, Y.; Elkashlan, M.; Nallanathan, A. Resource Allocation for Secure URLLC in Mission-Critical IoT Scenarios. *IEEE Trans. Commun.* **2020**, *68*, 5793–5807. [[CrossRef](#)]
13. Nasir, A.A.; Tuan, H.D.; Ngo, H.Q.; Duong, T.Q.; Poor, H.V. Cell-Free Massive MIMO in the Short Blocklength Regime for URLLC. *IEEE Trans. Wirel. Commun.* **2021**, *20*, 5861–5871. [[CrossRef](#)]
14. Lin, X.; Zhu, X.; Jiang, Y.; Cao, J. Pilot Overhead vs. Pilot Power: Short Packet Structure Optimization for URLLC over Continuous Fading. In Proceedings of the 2021 IEEE Global Communications Conference (GLOBECOM), Madrid, Spain, 7–11 December 2021; pp. 01–06.
15. Zhang, X.; Zhang, D.; Shim, B.; Han, G.; Zhang, D.; Sato, T. Sparse Superimposed Coding for Short Packet URLLC. *IEEE Internet Things J.* **2021**, *9*, 5275–5289. [[CrossRef](#)]
16. Östman, J.; Lancho, A.; Durisi, G.; Sanguinetti, L. URLLC With Massive MIMO: Analysis and Design at Finite Blocklength. *IEEE Trans. Wirel. Commun.* **2021**, *20*, 6387–6401. [[CrossRef](#)]
17. Cao, J.; Zhu, X.; Jiang, Y.; Liu, Y.; Wei, Z.; Sun, S.; Zheng, F.C. Independent Pilots vs. Shared Pilot: Short Frame Structure Optimization for Heterogeneous-Traffic URLLC Networks. *IEEE Trans. Wirel. Commun.* **2022**, *1*. [[CrossRef](#)]
18. Brik, V.; Banerjee, S.; Gruteser, M.; Oh, S. Wireless device identification with radiometric signatures. In Proceedings of the 14th ACM International Conference on Mobile Computing and Networking, San Francisco, CA, USA, 13–19 September 2008; pp. 116–127.
19. Nguyen, N.T.; Zheng, G.; Han, Z.; Zheng, R. Device fingerprinting to enhance wireless security using nonparametric Bayesian method. In Proceedings of the 2011 Proceedings IEEE INFOCOM. Shanghai, China, 10–15 April 2011; pp. 1404–1412.
20. Restuccia, F.; D’Oro, S.; Melodia, T. Securing the internet of things in the age of machine learning and software-defined networking. *IEEE Internet Things J.* **2018**, *5*, 4829–4842. [[CrossRef](#)]
21. Lee, D.H.; Lee, I.Y. Dynamic group authentication and key exchange scheme based on threshold secret sharing for Iot smart metering environments. *Sensors* **2018**, *18*, 3534. [[CrossRef](#)]
22. Xu, Q.; Zheng, R.; Saad, W.; Han, Z. Device fingerprinting in wireless networks: Challenges and opportunities. *IEEE Commun. Surv. Tutor.* **2015**, *18*, 94–104. [[CrossRef](#)]
23. Al-Shawabka, A.; Restuccia, F.; D’Oro, S.; Jian, T.; Rendon, B.C.; Soltani, N.; Dy, J.; Ioannidis, S.; Chowdhury, K.; Melodia, T. Exposing the fingerprint: Dissecting the impact of the wireless channel on radio fingerprinting. In Proceedings of the IEEE INFOCOM 2020-IEEE Conference on Computer Communications, Beijing, China, 27–30 April 2020; pp. 646–655.
24. Gritsenko, A.; Wang, Z.; Jian, T.; Dy, J.; Chowdhury, K.; Ioannidis, S. Finding a ‘New’ needle in the haystack: unseen radio detection in large populations using deep learning. In Proceedings of the 2019 IEEE International Symposium on Dynamic Spectrum Access Networks (DySPAN), Newark, NJ, USA, 11–14 November 2019; pp. 1–10.
25. Jian, T.; Rendon, B.C.; Ojuba, E.; Soltani, N.; Wang, Z.; Sankhe, K.; Gritsenko, A.; Dy, J.; Chowdhury, K.; Ioannidis, S. Deep learning for RF fingerprinting: A massive experimental study. *IEEE Internet Things Mag.* **2020**, *3*, 50–57. [[CrossRef](#)]
26. Peng, L.; Hu, A.; Zhang, J.; Jiang, Y.; Yu, J.; Yan, Y. Design of a hybrid RF fingerprint extraction and device classification scheme. *IEEE Internet Things J.* **2018**, *6*, 349–360. [[CrossRef](#)]
27. Le, K.N. URLLC Performance Under Outdated Channel State Information and Generalised-Rician Fading. *IEEE Trans. Veh. Technol.* **2021**, *70*, 12174–12178. [[CrossRef](#)]
28. Xiao, C.; Zeng, J.; Ni, W.; Su, X.; Liu, R.P.; Lv, T.; Wang, J. Downlink MIMO-NOMA for ultra-reliable low-latency communications. *IEEE J. Sel. Areas Commun.* **2019**, *37*, 780–794. [[CrossRef](#)]
29. Soltanieh, N.; Norouzi, Y.; Yang, Y.; Karmakar, N.C. A review of radio frequency fingerprinting techniques. *IEEE J. Radio Freq. Identif.* **2020**, *4*, 222–233. [[CrossRef](#)]
30. LeCun, Y.; Bengio, Y.; Hinton, G. Deep learning. *Nature* **2015**, *521*, 436–444. [[CrossRef](#)] [[PubMed](#)]
31. Zhang, T.; Ren, P.; Ren, Z. Deep Radio Fingerprint ResNet for Reliable Lightweight Device Identification. In Proceedings of the 2021 IEEE 94th Vehicular Technology Conference (VTC2021-Fall), Norman, OK, USA, 27–30 September 2021; pp. 1–6.
32. Huynh-The, T.; Nguyen, T.V.; Pham, Q.V.; Kim, D.S.; Da Costa, D.B. MIMO-OFDM Modulation Classification Using Three-Dimensional Convolutional Network. *IEEE Trans. Veh. Technol.* **2022**, *1*. [[CrossRef](#)]
33. Peng, S.; Jiang, H.; Wang, H.; Alwageed, H.; Zhou, Y.; Sebdani, M.M.; Yao, Y.D. Modulation Classification Based on Signal Constellation Diagrams and Deep Learning. *IEEE Trans. Neural Netw. Learn. Syst.* **2019**, *30*, 718–727. [[CrossRef](#)]
34. Pham, H.; Dai, Z.; Xie, Q.; Luong, M.T.; Le, Q.V. Meta pseudo labels. *arXiv* **2020**, arXiv:2003.10580.
35. O’shea, T.; Hoydis, J. An introduction to deep learning for the physical layer. *IEEE Trans. Cogn. Commun. Netw.* **2017**, *3*, 563–575. [[CrossRef](#)]

36. Arazo, E.; Ortego, D.; Albert, P.; O'Connor, N.E.; McGuinness, K. Pseudo-labeling and confirmation bias in deep semi-supervised learning. In Proceedings of the 2020 International Joint Conference on Neural Networks (IJCNN), Scotland, UK, 19–24 July 2020; pp. 1–8.
37. He, K.; Zhang, X.; Ren, S.; Sun, J. Identity mappings in deep residual networks. In Proceedings of the European Conference on Computer Vision, Amsterdam, The Netherlands, 11–14 October 2016; Springer: Berlin/Heidelberg, Germany, 2016; pp. 630–645.
38. Lapidoth, A.; Shamai, S. Fading channels: how perfect need “perfect side information” be? In Proceedings of the 1999 IEEE Information Theory and Communications Workshop, Kruger National Park, South Africa, 20–25 June 1999; pp. 36–38.
39. Martinez, A.; i Fàbregas, A.G. Saddlepoint approximation of random-coding bounds. In Proceedings of the 2011 Information Theory and Applications Workshop, San Diego, CA, USA, 2–7 February 2011; pp. 1–6.
40. O’Shea, Timothy James.; Roy, Tamoghna.; Clancy, T. Charles. Over-the-Air Deep Learning Based Radio Signal Classification. *IEEE J. Sel. Top. Signal Process.* **2018**, *12*, 168–179. [[CrossRef](#)]
41. Jian, T.; Gong, Y.; Zhan, Z.; Shi, R.; Soltani, N.; Wang, Z.; Dy, J.G.; Chowdhury, K.R.; Wang, Y.; Ioannidis, S. Radio Frequency Fingerprinting on the Edge. *IEEE Trans. Mob. Comput.* **2021**, *99*, 1. [[CrossRef](#)]
42. Vu, Thai-Hoc and Nguyen, Toan-Van and Nguyen, Tien-Tung and Kim, Sunghwan Performance Analysis and Deep Learning Design of Wireless Powered Cognitive NOMA IoT Short-Packet Communications with Imperfect CSI and SIC. *IEEE Internet Things J.* **2021**, *1*, 1. [[CrossRef](#)]
43. Björnson, E.; Hoydis, J.; Sanguinetti, L. Massive MIMO Networks: Spectral, Energy, and Hardware Efficiency. *Found. Trends Signal Process.* **2017**, *11*, 54–655. [[CrossRef](#)]